Journal of Applied Physics

Room temperature exchange bias in antiferromagnetic composite $BiFeO_3$-$TbMnO_3$

Cite as: J. Appl. Phys. **126**, 243903 (2019); https://doi.org/10.1063/1.5109713
Submitted: 14 May 2019 . Accepted: 03 December 2019 . Published Online: 24 December 2019

Prince K. Gupta, Surajit Ghosh, Shiv Kumar, Arkadeb Pal, Prajyoti Singh, Mohd Alam, Abhishek Singh, Somnath Roy, Rahul Singh, Bheeshma Pratap Singh, N. Naveen Kumar, Eike F. Schwier, Masahiro Sawada, Takeshi Matsumura, Kenya Shimada, Hong-Ji Lin, Yi-Ying Chin, A. K. Ghosh, and Sandip Chatterjee

Journal of Applied Physics ARTICLE scitation.org/journal/jap

Room temperature exchange bias in antiferromagnetic composite $BiFeO_3$-$TbMnO_3$

Cite as: J. Appl. Phys. **126**, 243903 (2019); doi: 10.1063/1.5109713
Submitted: 14 May 2019 · Accepted: 3 December 2019 ·
Published Online: 24 December 2019

Prince K. Gupta,[1] Surajit Ghosh,[1] Shiv Kumar,[2] Arkadeb Pal,[1] Prajyoti Singh,[1] Mohd Alam,[1] Abhishek Singh,[1] Somnath Roy,[3] Rahul Singh,[4] Bheeshma Pratap Singh,[5] N. Naveen Kumar,[6] Eike F. Schwier,[2] Masahiro Sawada,[2] Takeshi Matsumura,[2] Kenya Shimada,[2] Hong-Ji Lin,[7] Yi-Ying Chin,[8] A. K. Ghosh,[3] and Sandip Chatterjee[1,a)]

AFFILIATIONS

[1]Department of Physics, Indian Institute of Technology (BHU) Varanasi, Varanasi 221005, Uttar Pradesh, India
[2]Hiroshima Synchrotron Radiation Center, Hiroshima University, Kagamiyama 2-313, Higashi-Hiroshima 739-0046, Japan
[3]Department of Physics, Banaras Hindu University, Varanasi 221005, Uttar Pradesh, India
[4]Solid State Physics Division, Bhabha Atomic Research Centre, Trombay, Mumbai 400085, India
[5]Chemistry Division, Bhabha Atomic Research Centre, Trombay, Mumbai 400085, India
[6]Material Science Division, Bhabha Atomic Research Centre, Trombay, Mumbai 400085, India
[7]National Synchrotron Radiation Research Center, Hsinchu 300, Taiwan
[8]Department of Physics, National Chung Cheng University, 168, Sec. 1, University Road, Min-Hsiung, Chiayi 62102, Taiwan

[a)]**Author to whom correspondence should be addressed:** schatterji.app@iitbhu.ac.in

ABSTRACT

The magnetic property of a $0.7BiFeO_3$-$0.3TbMnO_3$ composite has been studied in detail and compared with that of $0.8BiFeO_3$-$0.2TbMnO_3$. The magnetic properties in $0.7BiFeO_3$-$0.3TbMnO_3$ are improved in manifold compared to $BiFeO_3$. An exchange bias (H_{EB}) is observed in both the compositions of these antiferromagnetic composites, which varies between 5 and 180 Oe with a maximum at ~275 K. Isothermal remanent magnetization measurements at room temperature indicate the presence of an interfacial layer of a 2-dimensional dilute uniaxial antiferromagnet in a uniform magnetic field (2D DAFF). The presence of exchange bias can be explained on the basis of a strong strain-mediated magnetoelectric coupling induced exchange interaction and the creation of a 2D DAFF layer at the interface. The properties of this layer are defined by canting and pinning of $BiFeO_3$ spins at the interface with $TbMnO_3$ due to Fe and Mn interaction. X-ray magnetic circular dichroism confirms the presence of canted antiferromagnetic ordering of $BiFeO_3$, charge transfer between Mn ions, and different magnetically coupled layers that play a vital role in the exchange bias.

I. INTRODUCTION

Since its discovery by Meiklejohn and Bean in 1956, the exchange bias (EB) phenomenon has been the focus of extensive theoretical and experimental analysis, and more recently, it is attracting researchers for its potential application in devices like giant magnetoresistance, high-density data storage, electrically controllable spin-polarized currents, magnetic sensors, and spin valve devices.[1–3] Conventional exchange bias is observed at the interface between ferromagnetic (FM) and antiferromagnetic (AFM) materials when cooled in a field through the Néel temperature (T_N) of the hard magnetic material.[1–3] Apart from interacting interfaces between FM and AFM materials, the effect has so far been observed in different types of heterostructures, such as ferromagnetic–antiferromagnetic, ferromagnetic–spin glass–antiferromagnetic, ferromagnetic–ferrimagnetic, ferromagnetic–dilute antiferromagnetic, etc., and in different geometries like bilayers, core-shell nanostructures, granular composites, and superlattices.[2–6]

In recent years, $BiFeO_3$ (BFO) has emerged as one of the most significant materials for investigating the EB and multiferroicity. It is the only perovskite material that shows multiferroic behavior at room temperature (Néel temperature $T_N \approx 643$ K and Curie temperature $T_C \approx 1100$ K).[7] Different low-dimensional BFO systems,

such as nanoparticles and nanotubes, are known to display weak ferromagnetic behavior at room temperature and spin glass-type behavior at low temperature.[8–10] The EB and its origin in BFO based systems are in discussion in recent times.[6,8,11–16] It was found to persist at room temperature in some nanodimensional systems consisting of BFO and was ascribed to the spin pinning at the interface between the AFM and weak FM layers present in those structures.[8] Dong *et al.* have demonstrated that EB exists in BFO nanocrystals with a nonmonotonic temperature dependence of H_{EB}. They proposed that the formation of a diluted antiferromagnetic phase and its interaction with the hard AFM moments was the mechanism responsible for the high-temperature behavior of H_{EB}. The low-temperature H_{EB} was explained by suggesting the formation of cluster spin glass-type structure and related interactions.[11] Cluster glass (CG) (clusters of glass phases) and superspin glass (SSG) (a glass phase of ferromagnetic or ferrimagnetic single domain nanoparticles) structures are crucial in explaining exchange bias in different systems.[17,18] Manna *et al.* have reported H_{EB} above the superspin glass (SSG) transition within their $BiFe_{0.8}Mn_{0.2}O_3$ nanoparticles and have explained the EB on the basis of interaction between antiferromagnetic core and a diluted uniaxial antiferromagnet in a uniform magnetic field (DAFF) shell.[12] Zhang *et al.* have also shown room temperature exchange bias in BFO nanocrystals and explained the phenomenon as a consequence of interaction between antiferromagnetic core and DAFF shell.[16] Recently, Maity *et al.*, on the other hand, found EB only when an SSG-type structure is formed at low temperature in $BiFeO_3$-$Bi_2Fe_4O_9$ nanostructures, and the phenomenon was linked to pinning of glassy spins to the remaining antiferromagnetic spins.[14,16] A skin layer different from its bulk is also reported in single crystalline BFO, which influences several of its properties including the EB.[19]

Several attempts have been made to induce chemical pressure in the BFO lattice by substituting Bi or Fe ions with rare earth and transition metal (TM) atoms. Substitution is known to modify the magnetic behavior and enhance the EB.[15]Attempts have also been made to integrate BFO in heterostructures and composite systems containing other perovskite materials like $BaTiO_3$ and $SrTiO_3$.[20,21] However, a clear understanding of the mechanism that leads to the EB effect is still missing. Although the EB effect has been investigated for many years, obtaining a large H_{EB} at room temperature and within the bulk state remains an ongoing task since room temperature EB is more attractive for device applications.

In this context, we decided to incorporate $TbMnO_3$ [TMO; which shows very strong magnetoelectric (ME) coupling] into $BiFeO_3$. $TbMnO_3$ (TMO) is a promising material to induce strain at the single phase interfaces in the system.[22] TMO possesses a perovskite structure (space group *Pbnm*), and the lattice mismatch between the two materials in the composite system is sufficient to create strain.[22] In this article, we have investigated composites of 0.7BFO-0.3TMO (70% $BiFeO_3$ and 30% $TbMnO_3$) and 0.8BFO-0.2TMO (80% $BiFeO_3$ and 20% $TbMnO_3$). It is observed that with increasing TMO content magnetic properties enhanced, and in 0.7BFO-0.3TMO, the enhancement is larger than that in 0.8BFO-0.2TMO. We have mainly discussed the results of 0.7BFO-0.3TMO composite to explain the origin of exchange bias in this composite, and we have also compared the results with that of 0.8BFO-0.2TMO. Further, we have demonstrated by means of x-ray magnetic circular dichroism (XMCD) that the canted nature of antiferromagnetic ordering in BFO, exchange interaction between Fe and Mn ions, and the pinning layer at the interface play a vital role in determining the amplitude and temperature behavior of the EB.

II. EXPERIMENTAL METHODS

The synthesis of magnetoelectric multiferroics composite consisting of $BiFeO_3$ via solid state reaction is a difficult task because it commonly leads to the formation of thermodynamically stable impurities $Bi_2Fe_4O_9$, $Bi_{25}FeO_{39}$, and $Bi_{46}Fe_2O_{72}$ due to the volatile nature of Bi_2O_3.[23] In this work, we have used high purity oxides Bi_2O_3, Fe_2O_3, Mn_2O_3, and Tb_4O_7 as starting materials. First, polycrystalline $TbMnO_3$ was prepared through a solid state reaction as described in a previous report.[24] Then, stoichiometric amounts of the materials Bi_2O_3 (5% excess), Fe_2O_3, and $TbMnO_3$ were mixed and ground for 3–4 h, and then, the mixture was calcined at 1173 K for 1 h to prepare composites with two different ratios (7:3 and 8:2). The calcined powder was ground and pressed into pellets and sintered for 2 h at 1273 K with some mixture of calcined powder as a spacer to reduce the loss of Bi_2O_3 during synthesis.

The structural analysis of the composite was carried out using an X-ray diffractometer (Model: Miniflex-II, Rigaku, Japan) with Cu Kα radiation ($\lambda = 1.5406$ Å) in step size of 0.002 with a scan speed of 2°/min. The microstructures were also studied from transmission electron microscopy (TEM). The microstructure was further analyzed using transmission electron microscopy (TEM) images of samples that were recorded via a Jeol 2000 FX. The samples were characterized by atomic and magnetic force microscopy (AFM/MFM) for its morphology and magnetic domain structure study using NT-MDT, Russia. The images were analyzed using software, namely, Nova-Px for the sectional and roughness analysis. The magnetic properties were investigated using a commercial superconducting quantum interference device (Magnetic Properties Measurement System XL-7, Quantum Design, Inc.) magnetometer. X-ray absorption spectroscopy (XAS) and x-ray magnetic circular dichroism (XMCD) measurements at Mn $L_{2,3}$-edge and Fe $L_{2,3}$-edge at 300 K and 180 K were performed with polarized x-rays at beamline from Hsinchu Synchroton center, Taiwan.

III. RESULTS AND DISCUSSION

A. Structure and morphology

Figures 1(a) and 1(b) show the refinement of the x-ray diffraction profile for the composites 0.7BFO-0.3TMO and 0.8BFO-0.2TMO, respectively, in the 2θ range from 20° to 80°. A close look at the 2θ value of 32° that corresponds to the 110 plane of BFO in an *R3c* phase reveals that the peak is shifted to the higher angle side as well as split into multiple peaks, which hints toward the existence of multiple phases of BFO. LeBail refinement using the FULLPROF package was employed to index the XRD pattern for analyzing the crystal structure and structural phase transition from the intensities of overlapping reflections in the XRD pattern. The difference between experimental and theoretical patterns as well as Bragg positions are shown in the bottom of the plot. From the refinement result, it was found that in the composite, TMO crystallizes as in its native bulk structure, i.e., orthorhombically distorted perovskite structure with space group

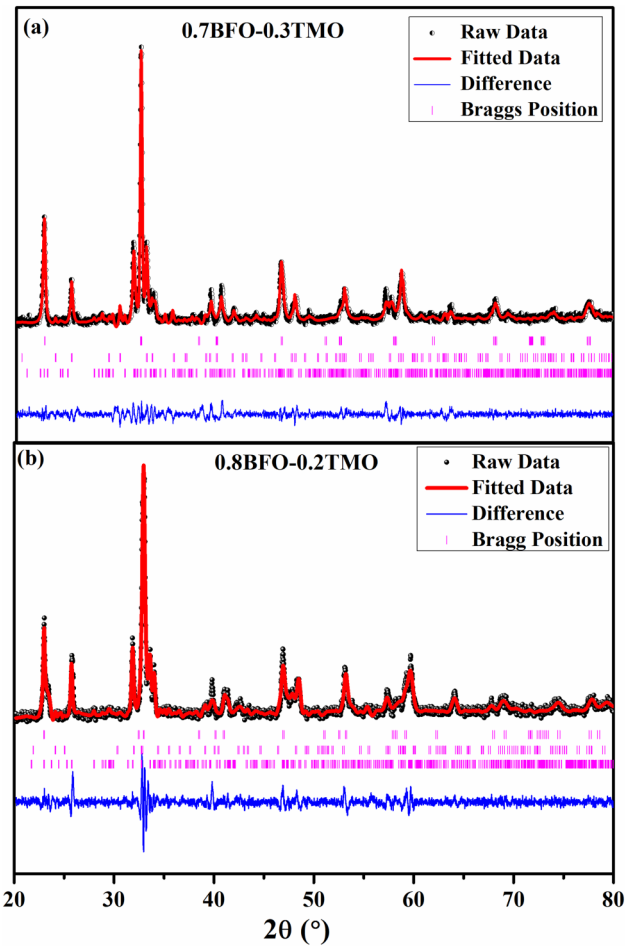

FIG. 1. LeBail refinement of the XRD data of the composites (a) 0.7BFO-0.3TMO and (b) 0.8BFO-0.2TMO. The top set of Bragg's positions represents the *R3c* phase of $BiFeO_3$. Middle set of Bragg's positions shows the *Pbnm* phase of $TbMnO_3$, and the bottom set of Bragg's positions shows the *Pbnm* phase of $BiFeO_3$.

Pbnm. BFO on the other hand is found to coexist in two very similar phases consisting of rhombohedral and orthorhombic symmetries (*R3c* + *Pbnm*). The refinement results (lattice parameters) are given in Table I from which it can be seen that the parameters are in well accordance with those reported earlier.[25–27] The crystalline size was also calculated to be ~63 nm and 60 nm for 0.7BFO-0.3TMO and 0.8BFO-0.2TMO, respectively. It is also clear from Table I that the lattice parameters of the individual phases are considerably different for 0.7BFO/0.3TMO and 0.8BFO/0.3TMO, which reflects the complex chemical nature of the phases.

Rare earth orthoferrites $RFeO_3$ (*R* = rare earth), manganites, and the high-temperature phase of BFO are known to undergo a structural transition from the rhombohedral *R3c* structure to an orthorhombic (*Pnma* or *Pbnm*) structure when sintered at higher temperature.[28] The observation of the existence of dual phases, i.e., rhombohedral (*R3c*) and orthorhombic (*Pnma or Pbnm*), in rare earth (RE)-modified BFO has previously been reported.[29] Recent reports show that BFO in solid solution with rare earth manganites ($RMnO_3$), i.e., $BiFeO_3$-$RMnO_3$ (*R* = La, Gd, Ho, and Dy), and (1 − x) $BiFeO_3$-x$YMnO_3$ undergo a structural phase transition from *R3c* to *R3c* + *Pnma* over a wide compositional range.[30,31] This structural transition to dual phases was accompanied by a significant improvement of multiferroic properties within BFO. Lotey and Verma reported complete structural transformation from rhombohedral (*R3c*) to the orthorhombic ($Pn2_1a$) phase at 15% of Tb-doping in BFO nanoparticles.[32] In the composite, the dual phase structure of $BiFeO_3$ can arise due to the smaller chemical pressure of Tb^{3+} than Bi^{3+} as the ionic radii of Bi^{3+} and Tb^{3+} are 1.31 Å and 1.17 Å, respectively. The deficiency of $6s^2$ lone pair in Tb^{3+} also hinders the stereochemical activity of the lone pair of Bi^{3+} ions destabilizing the structure.[33] The presence of Mn^{3+} ions in the structures is also known to weakly destabilize the *R3c* phase, whereas Fe^{3+} is known to stabilize it.[33] The two phases in our sample correspond to bulk (*R3c*) and interfacial (*Pbnm*) phases at the interface with $TbMnO_3$. The interfacial regions of the $BiFeO_3$ crystals face strain due to the presence of Tb^{3+} and Mn^{3+}, and the interface structure changes to the *Pbnm* phase. Apart from these structural changes, high-temperature synthesis can also lead to oxygen deficiency and cation deficiency.

To further analyze the results obtained in XRD, we have characterized our sample with transmission electron microscopy (TEM) that is a very powerful technique used to study compositional, morphological, and crystallographic information of a sample. Figure 2 shows the typical TEM image of a uniformly dispersed magnetoelectric composite 0.7BFO-0.3TMO and their selected area electron diffraction (SAED) patterns. Figure 2(a) shows that two types of morphology of particles having spherical and cubical shapes correspond to BFO and TMO, respectively. We can safely assume that the spherical and cubical shapes belong to BFO and TMO, respectively; as in earlier studies, the TEM morphology of the BFO particles has been reported as spherical, whereas that of TMO has been reported as cubical [indicated in Fig. 2(a)].[34,35] In order to determine the particle size of the composite, the TEM images with more particles have been recorded as shown in Fig. 2(b). The selected area electron diffraction (SAED) patterns of both kinds of particles have been recorded and are shown in Figs. 2(c) and 2(d). The presence of sharp diffraction spots in a regular circle manifests that the composite is well crystallized. These diffraction spots belong to different Miller planes of a rhombohedral structure of $BiFeO_3$ and indexed with the help of their x-ray diffraction data. Similar procedure is adopted for the SAED pattern of TMO and indexed with their Miller planes. A close view [Fig. 2(e)] of the circular particles, i.e., BFO particles, reveals that apart from the core particle there is also a thin skinlike layer. The inner and outer periferi of the particles are marked with blue and maroon arrows in the figure. This interfacial layer must correspond to the *Pbnm* phase observed in the XRD. Furthermore, the size distribution curve for the present sample is generated using Image J software and is shown in Fig. 2(f). The average particle size of the composites, determined by employing fitting of Gaussian distribution function, was found to be 11.85 nm.

In order to visualize the surface morphology and magnetic structure, AFM and corresponding MFM measurements of the

TABLE I. Refinement results (lattice parameter) of 0.7BFO-0.3TMO and 0.8BFO-0.2TMO composites.

0.7BFO-00.3TMO			
Parameters/sample	$BiFeO_3$ (BFO)		$TbMnO_3$ (TMO)
	Phase-I	Phase-II	
Crystal structure	Rhombohedral	Orthorhombic	Orthorhombic
Space group	R3c	Pnma	Pbnm
Lattice parameters (A°)			
a	5.5132	5.6013	5.31398
b	5.5132	15.6400	5.8765
c	13.4614	11.2515	7.4366
α	90°	90°	90°
β	90°	90°	90°
ϒ	120°	90°	90°
Crystalline size (nm)		63.0	
Density (g/cm^3)		8.01	
0.8BFO-0.2TMO			
Parameters/sample	$BiFeO_3$ (BFO)		$TbMnO_3$ (TMO)
	Phase-I	Phase-II	
Crystal structure	Rhombohedral	Orthorhombic	Orthorhombic
Space group	R3c	Pnma	Pbnm
Lattice parameters (A°)			
a	5.5176	5.3336	5.5990
b	5.5176	15.4884	5.8932
c	13.2161	11.2344	7.3793
α	90°	90°	90°
β	90°	90°	90°
ϒ	120°	90°	90°
Crystalline size (nm)		60.30	
Density (g/cm^3)		7.77	

sintered 0.7BFO-0.3TMO composite were performed. Figures 3(a) and 3(b) show the AFM and the corresponding MFM image of the composite over a surface area of $10 \times 10\,\mu m^2$, respectively. It is clear from figure that the composite exhibits a grainylike surface with uniformly and nonhomogenously distributed grains. The average grain size was calculated by line scan sectional analysis to be of ∼180 nm, which is consistent with the crystallite size calculated from the XRD pattern. Further, the composite also displays larger grains growth due to the agglomeration of smaller grains.[36]

The corresponding MFM image that was taken at a lift height of 200 nm is presented in Fig. 3(b). From the figure, disappearance of grains can be seen as compared to the AFM image of the composite, and contrasting dark and bright images were found to display the domain structure. Since short range attractive and repulsive forces between the sample and magnetic tip create the light and dark contrast areas, these spots can be considered to correspond to the magnetic domains of the composite.[36,37] Thus, from the image, very small domains can be seen, which is obvious for the antiferromagnetic materials.[36–38] The surface of the grains, thus, appeared to be antiferromagnetic in nature. The average domain size and the magnetic signal strength were calculated using the sectional scan analysis.

B. Magnetic properties

Figures 4(a) and 4(b) depict the temperature dependence of field cooling (FC) and zero field cooling (ZFC) dc-magnetization for composites 0.7BFO-0.3TMO and 0.8BFO-0.2TMO, respectively. The two different compositions show similar behaviors in the ZFC-FC magnetization, where the ZFC and FC values increase with decreasing temperature at low temperatures. In this plot [Fig. 4(a)], the magnetization (both FC and ZFC) for the composition 0.7BFO-0.3TMO is observed to decrease with decreasing temperature in the temperature range of 215–300 K, which is expected for an antiferromagnetic material below its Néel temperature. Further, on decreasing the temperature below 215 K, FC and ZFC magnetization curves show upturns. To get a clear view of the anomaly, the dM/dT vs T is plotted in the insets of the Figs. 4(a) and 4(b) from where it is found that in the case of 0.7BFO-0.3TMO the slope of the dM/dT vs T curves changes abruptly at ∼215 K, whereas for the other composite, the transition temperature was found to be 169 K. Similar trends have previously been reported as a result of reorientations of spins with the involvement of electromagnons, as is observed in orthoferrites.[39–41] The transition is reported to be of magnetic origin and not related to structural deformation or transition.[41] Although the spin reorientation transition

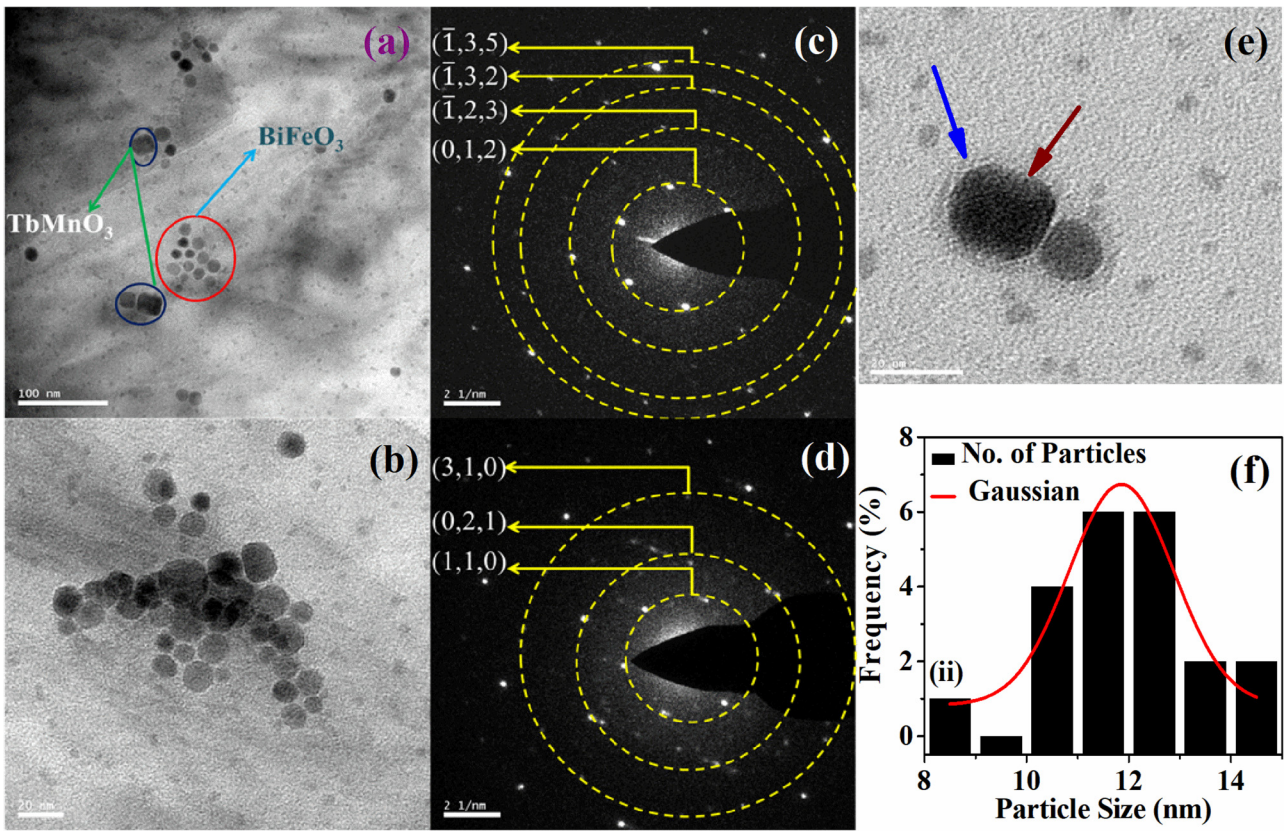

FIG. 2. (a) and (b) The TEM image of the 0.7BFO-0.3TMO composite showing BFO and TMO particles. (c) and (d) SAED patterns of BFO and TMO particles. (e) Close view of the interfacial layer of BFO particles. Blue and maroon arrows indicate the core and interfacial layer. (f) Particle size distribution of the 0.7BFO-0.3TMO composite.

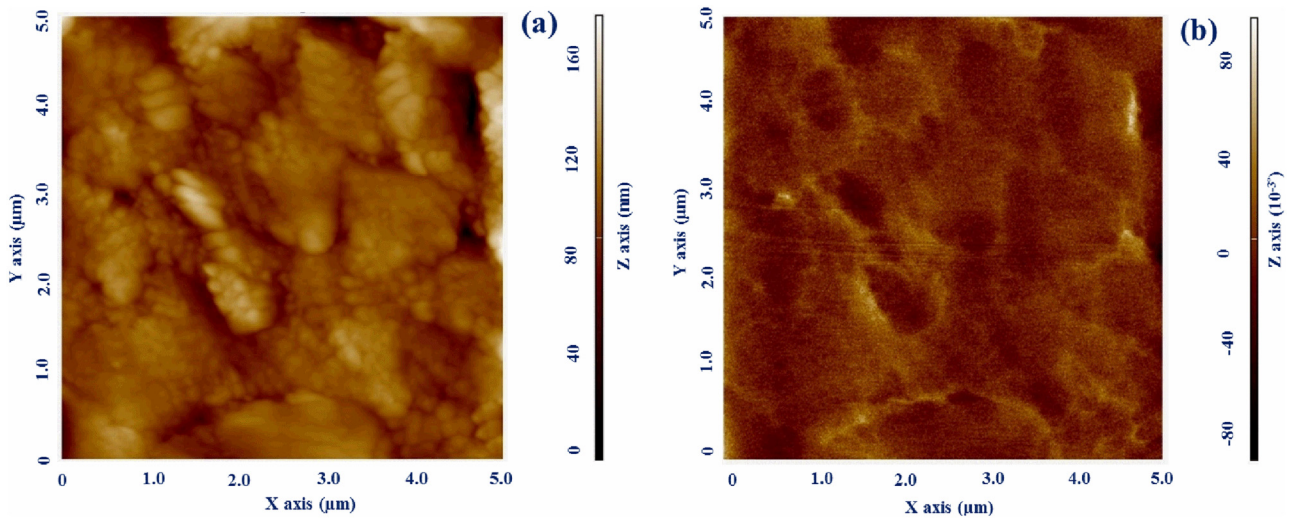

FIG. 3. (a) AFM and (b) MFM image of the 0.7BFO-0.3TMO composite.

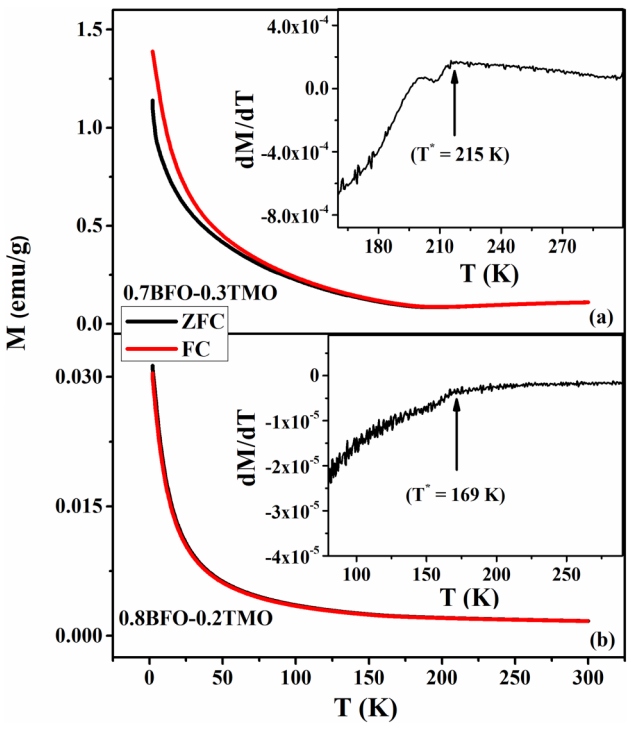

FIG. 4. ZFC and FC magnetization vs temperature plots for (a) 0.7BFO-0.3TMO and (b) 0.8BFO-0.2TMO composites under an applied magnetic field of 1000 Oe. Inset: the dM/dT vs T plots for the respective sample. The arrows in the insets point toward the spin reorientation transition temperature T*.

is reported well above the room temperature and just below the T_N for different composite systems such as $BiFeO_3$-$PbTiO_3$ and $BiFeO_3$-$BaTiO_3$, the spin reorientation transition temperature (T*) has been reported in the temperature range of 150–200 K for pure $BiFeO_3$.[40,41] Recently, Kumar and Pandey have also observed such a spin reorientation transition in pure and 0.3% MnO_2 doped $BiFeO_3$ powders in the same temperature range.[41] The transition is similar in nature with the Morin transition observed in α-Fe_2O_3. α-Fe_2O_3 shows canted antiferromagnetic nature above the transition, and below the transition it shows pure antiferromagnetic behavior. Kumar and Pandey performed neutron diffraction and studied extensively the spin configuration of $BiFeO_3$-$PbTiO_3$ composite at low temperatures below T_N.[41] They showed that configuration of Fe^{3+} spin in different layers can be expressed as G_{xz} and F_y, and below the spin reorientation, it shows G_y and F_{xz} ordering just like Morin transition observed in α-Fe_2O_3.[42,43] G and F represent G-type antiferromagnetic and ferromagnetic ordering in respective planes and directions. The spin reorientation is quite different from that observed in orthoferrites, which is driven by the coupling of two magnetic sublattices. Further decreasing the temperature, FC and ZFC magnetization curves of 0.7BFO-0.3TMO show very low bifurcation from 95 K to 2 K as the two curves deviate from each other very slowly toward lower temperatures. Although there is bifurcation in the plots, we have not found any traces of long range or short range ordering from either the dM/dT vs T plots or AC susceptibility measurements (not shown here) in both the samples. Moreover, as it is observed in Fig. 3(b), no bifurcation is observed in the FC and ZFC magnetization of 0.8BFO-0.2TMO. TMO is known to exhibit AFM ordering below 40 K in the bulk, but feature is also not traceable in M-T plots.[23]

Figure 5 presents the M-H loop of the composite 0.7BFO-0.3TMO at different temperatures after cooling from a higher temperature in the presence of a magnetic field 1 T. The M-H loop at room temperature shows a linear variation of magnetization with an applied magnetic field, which is typical for an antiferromagnetic material. Around the zero field, a deviation of nonlinearity is observed, which indicates the existence of FM ordering too. However, weak sigmoidal nature can be observed in M-H plots at 5 K that indicates some ferromagnetic contribution in the M-H plot at 5 K, which needs further study to understand the phenomenon. Furthermore, a close view around the zero field (insets a and b of Fig. 5) reveals that the loops, measured at 275 and 80 K, are asymmetric in nature, indicating the presence of exchange bias (EB) for 0.7BFO-0.3TMO at all the temperatures. The presence of loop shift in the M-H loop can be quantified as exchange bias field, $H_{EB} = [(H_{C1} + H_{C2})/2]$, where H_{C1} and H_{C2} are the points in the field axis where magnetization value becomes zero. The coercivity has also been estimated from the M-H loop as $H_C = [(H_{C1} - H_{C2})/2]$. H_{EB} estimated at different temperatures is plotted in Fig. 6 from which it becomes evident that H_{EB} exhibits clear temperature dependence. The measured exchange bias increases with an increase in the temperature from 5 K to 275 K. The similar variation in exchange bias has also been observed in 0.8BFO-0.2TMO composite (not shown). The temperature variation of exchange bias cannot be understood simply as generally exchange bias increases at low temperatures. To understand the observed exchange bias and its temperature variation, we have carried out following studies.

Recently, isothermal remanent magnetization (IRM) measurement is being used as a fingerprinting technique to differentiate among different magnetic states such as dilute uniaxial antiferromagnet in a uniform field (DAFF), spin glass, and others as it identifies the nature of the irreversible magnetization contributions.[44] We have performed IRM vs field measurements to check the presence of any interface pinning containing hard antiferromagnet BFO and possible dilute antiferromagnet. To measure the IRM, a field is applied for a very short duration (~60 s) after cooling it from a high temperature, and then the remanent magnetization is immediately recorded. It is expected that a pure AFM material will show zero IRM value for all fields and all temperatures as the reversible magnetization becomes zero for a pure AF state. In Fig. 7, it can be seen that the observed IRM value is very low and increases very slowly when the field is raised to 1.5 T where the virgin curve increases sharply and linearly with the field. This behavior is consistent with an AFM state. However, the IRM is not showing a typical behavior of a 3D dilute antiferromagnet as it is not expected to increase at all. This type of behavior of IRM has been found for Co_3O_4 nanowires where the nature of the particle is found to be of 2D DAFF.[45] The inset in Fig. 7 shows the temporal variation of the remanent magnetization of the composite 0.7BFO-0.3TMO after switching off an applied 1 T field. The zero

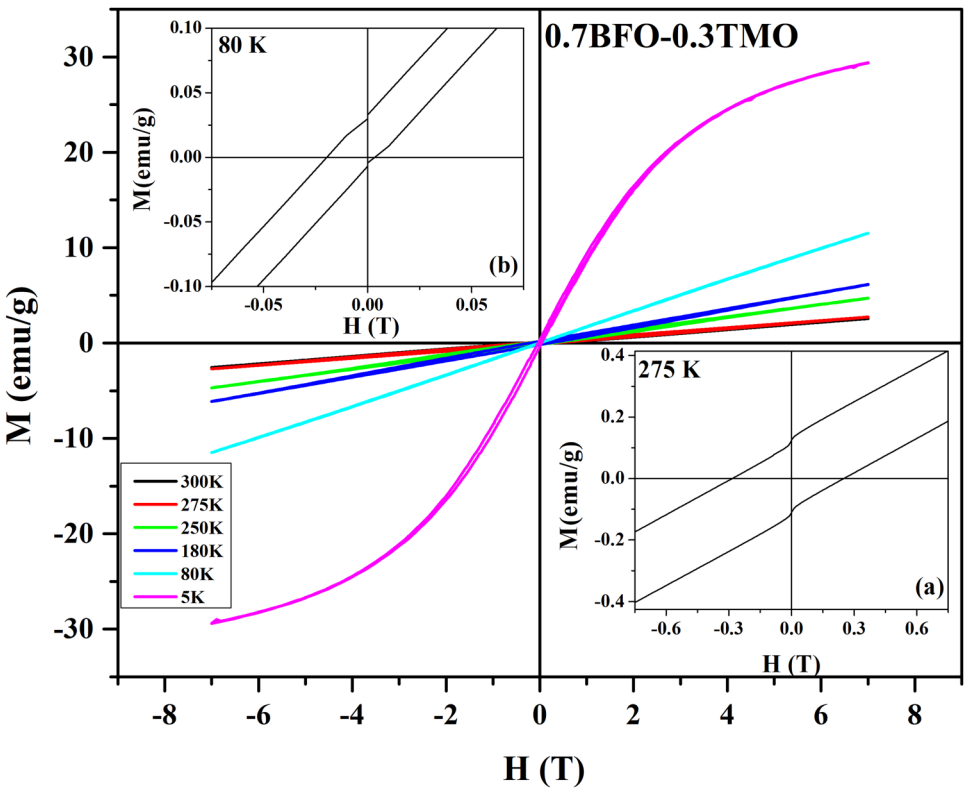

FIG. 5. The M-H loop of (a) 0.7BFO-0.3TMO and composite measured at different temperatures across 5–300 K after field cooling (1 T) from a higher temperature. Insets (a) and (b) show close view of the M-H loops around zero field measured at 275 K and 80 K, respectively.

point in the time axis stands for the moment when the magnetic field was switched off. The as-grown antiferromagnetic layer shows a net magnetization after a sufficient time of 1 h as an effect of uniform field applied to the DAFF layer.[46,47] The decay of the magnetization values can be seen to follow an logarithmic relation with temperature, which is also expected for the DAFF material.[46,47] Thus, the presence of DAFF layer in the composite is confirmed from these measurements. The 2D DAFF layer is attributed to the formation of a 2nd phase (*Pbnm*) of BFO at the interfacial regions other than that of core BFO (*R3c*). The antiferromagnetic ordering

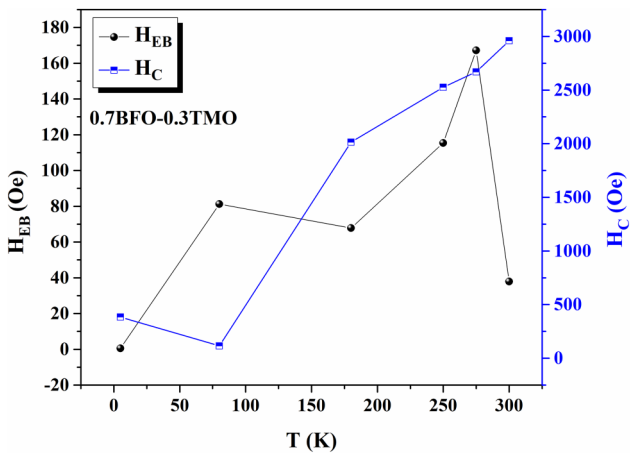

FIG. 6. The temperature dependence of exchange bias field (H_{EB}) and coercivity and (H_C) for 0.7BFO-0.3TMO.

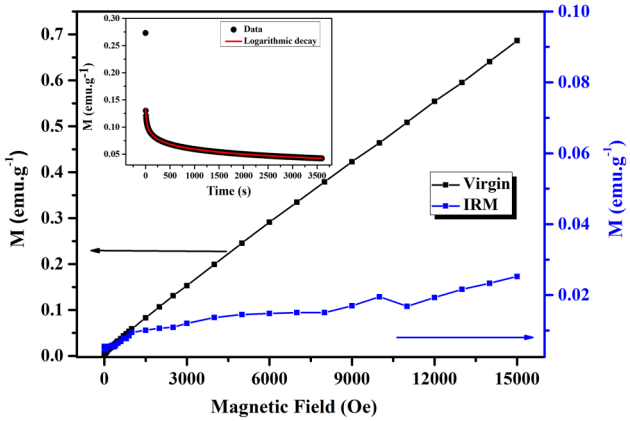

FIG. 7. Isothermal remnant magnetization (IRM) and the virgin loop of magnetization vs magnetic field of the composite 0.7BFO-0.3TMO. Inset shows the temporal variation of remanent magnetization of 0.7BFO-0.3TMO.

in the two phases is expected to be different.[19] However, the origin of the DAFF layer remains in doubt as it could be formed either due to the BFO skin layer or due to the TMO spins that could be coupled to the interfacial spins of the BFO.

The BFO/TMO interface is likely to be responsible for the EB and is expected to exhibit a complex interface structure, including charge transfer, atomic spin, and orbital configurations. At the interface of the composite, two different phases are combined at the atomic level, which results in an increased magnetoelectric (ME) coupling due to the strain-mediated ME effects across the interfaces.[48] This enhanced ME coupling can modify the lattice structure through spin reconstruction at the interface as is seen from the XRD results. From the calculation of magnetic coupling across the interface of $BiFeO_3$ and other manganites, it has been found that both charge and orbital ordering at the interface could result in developing a magnetic moment of Fe ions at the BFO-TMO interface.[13] Another possibility can be the presence of an orbital reconstruction that will lead to a strong hybridization between Fe $d_{3z2\text{-}r2}$ orbital and Mn $d_{x2\text{-}y2}$ via an oxygen mediated superexchange (SE).[3] According to the Anderson-Goodenough-Kanamori rules, the exchange interactions between Fe and Mn cations are expected to be ferromagnetic and the Mn-O-Mn interaction to be antiferromagnetic.[49] Thus, there lies a competition between the interfacial interaction of the Fe and Mn spins and the bulk antiferromagnetic interaction of the BFO, which results in the canting of the interfacial spins. The exchange bias can be understood to be due to the pinning and canting of the interfacial spins to the core antiferromagnetic spins of BFO. Moreover, the possibility of charge flow across the interface can be neglected as there is a large difference between the energy level of BFO and TMO, as estimated from atomic stacking $[(BiO)^+\text{-}(FeO_2)^-(BiO)^+\text{-}(MnO_2)\text{-}(TbO)^+]$ of BFO/TMO.[13,50] The strain-mediated ME coupling also produces a very thin layer of BFO with different structures as seen from the XRD and TEM results, which can be the reason behind the origin of 2D DAFF layer at the interface that also plays a significant role in the observed exchange bias. Thus, the large coercivity can also be explained on the basis of interfacial ferromagnetic superexchange interaction. At room temperature, the value of exchange bias is reduced from the maximum value at 275 K due to the large thermal fluctuations of spins resulting into less interfacial coupling.[11]

The origin of exchange bias in $BiFeO_3$ based systems has been an argued mechanism in recent years. As mentioned during the introduction, some $BiFeO_3$ based systems exhibit EB only below superspin glass (SSG) transition temperatures where the explanation was the presence of SSG moments.[6,14] The SSG moments at the core generate a random field that can induce a variation in the anisotropy of the AFM moments including biaxiality with respect to the direction of the applied field and set the uniaxial anisotropy via RKKY interaction.[14] It has already been shown (Fig. 4) that ZFC-FC M-T data show little bifurcation below ~95 K for 0.7BFO-0.3TMO suggesting weak frustration in the system, but in the case of 0.8BFO-0.2TMO, no bifurcation is observed in the ZFC-FC data. We also could not find signals of any relaxation phenomenon from our AC susceptibility measurements for both the samples (not shown here). Therefore, the possibility of any kind of SSG mediated phenomena that give rise to the EB effect can be ruled out. Thus, the results obtained from our study cannot be explained within the model given by Maity *et al.*[6,14] Manna *et al.* found room temperature and low temperature exchange bias in their Mn-doped BFO nanoparticles.[12] The results were understood on the basis of a core-shell model of hard antiferromagnetic core and dilute antiferromagnet shell where the spins of DAFF get pinned to the core's spins when a magnetic field is applied, thus setting the uniaxial anisotropy in the system. Zhang *et al.* also found the DAFF layer to influence the magnetic property of the $BiFeO_3$ nanoparticles.[16] Therefore, to verify the compatibility of this model with our system, a confirmation of type of interaction between the different ions present in the composite in different temperatures is necessary. To this end, we have recorded x-ray absorption (XAS) and x-ray magnetic circular dichroism (XMCD) spectra of Fe and Mn $L_{2,3}$ edges.

C. XAS and XMCD results

The synchrotron based XAS is a spectroscopic technique that probes electronic states of a matter. In x-ray absorption spectroscopy (XAS), x-ray is made incident on the core level electrons to excite them to unoccupied valence levels. The transition from core to valence level is governed by the dipole selection rules. Thus, XAS has direct correspondence with unoccupied density of states (DOS). As it has a direct correlation with the unoccupied density of states (DOS), several information regarding oxidation states, local symmetries, and the spin and orbital magnetic moments of the Fe and Mn ions and interaction between them in the composite can be investigated by means of XAS and XMCD measurements.

The XMCD signal at the Mn and Fe $L_{2,3}$ edges (excitation from filled $2p \rightarrow 3d$ transition) is obtained from the difference between the two XAS spectra, taken as the difference between XAS spectra recorded with left and right hand circularly polarized light ($\Delta\mu = \mu^+ - \mu^-$) in the presence of a magnetic field of 0.6 T. XMCD measurements were performed in the total electron yield (TEY) mode at 180 K and 300 K. Figures 8(a)–8(d) depict the XAS and XMCD spectra of Fe $L_{2,3}$ of the two composites measured at 300 K and 180 K. The spectral shape and energy position in the Fe $L_{2,3}$-edge splits due to spin-orbit coupling (SOC) at $L_3(2P_{3/2})$ at ~710 eV and L_2 $(2P_{1/2})$ at ~722 eV corresponding to the absorption edge of Fe^{3+} ions. The L_3 and L_2 peaks are also split due to the crystal field to doubly degenerate e_g and triply degenerate t_{2g} levels.[51] The shape of the XAS peak of BFO matches well with the Fe^{3+} signal previously seen in BFO based systems.[52,53] The shape of the spectral lines for the composites matches with the calculated spectrum taking the high spin configuration of Fe^{3+} ions ($t_{2g}^3e_g^2$) and with the measured Fe^{3+} XAS signal.[54] A closer look at the L_3 edge of the composites [the inset of Fig. 8(a)] when compared with the Fe L_3 edge of standard $\alpha\text{-}Fe_2O_3$ reveals that the spectral shape of the t_{2g} peak of the L_3 edge is diminished and shifted to the higher energy side for the composites. The overall spectra of the composites are also broader in comparison to $\alpha\text{-}Fe_2O_3$. These features of the t_{2g} can arise from the presence of either different crystalline coordination of the Fe ions or different valence states of Fe in the sample.[55,56] The L_2 edge of the composites shows Fe_3O_4-like diminished L_2 edge from where one might get the indication of the mixed valence state of Fe. But, a closer inspection of the L_2 edge [the inset of Fig. 8(b)] supports the fact that Fe ions are in

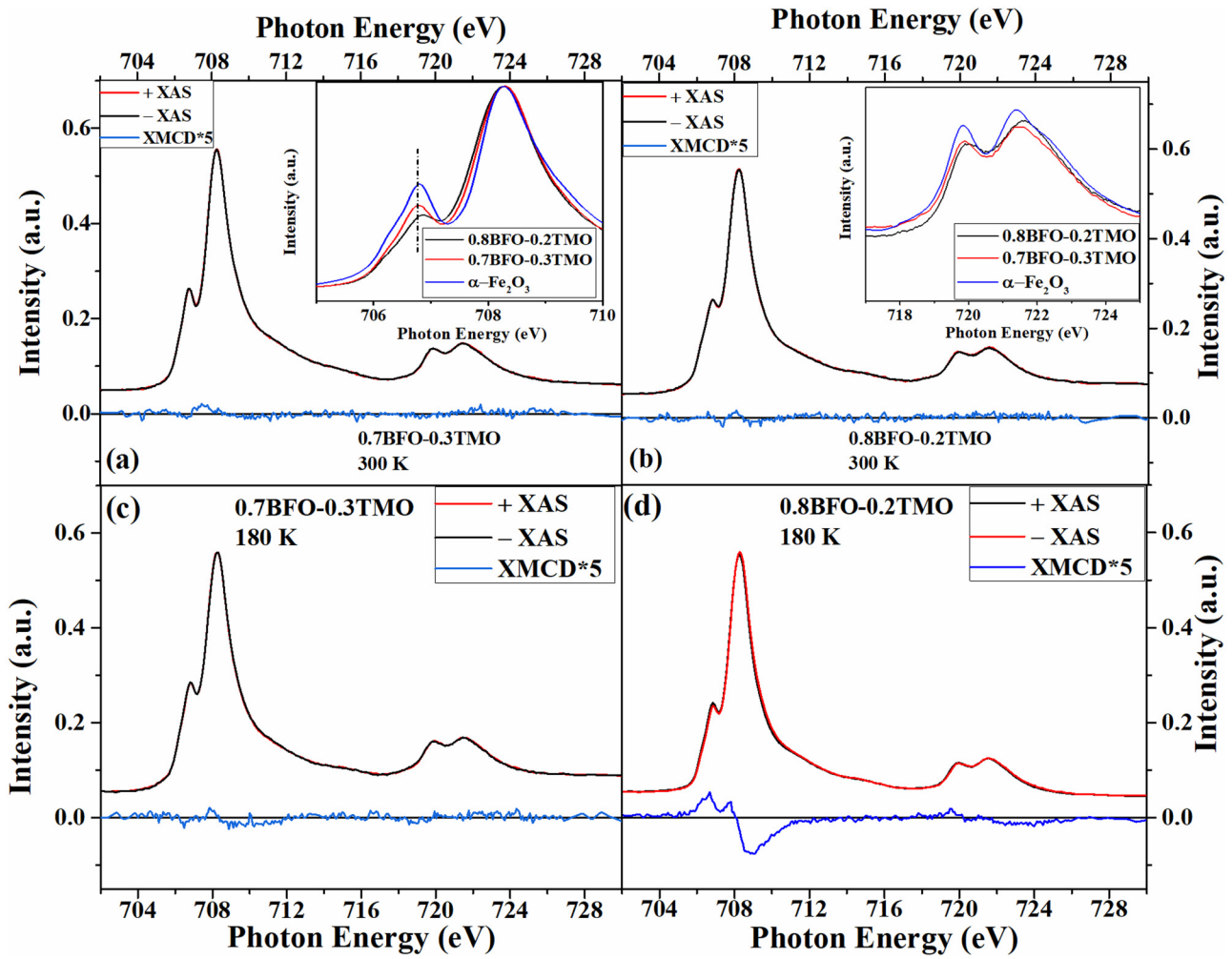

FIG. 8. Fe $L_{2,3}$ XAS and XMCD spectra of (a) 0.7BFO-0.3TMO at 300 K, (b) 0.8BFO-0.2TMO at 300 K, (c) 0.7BFO-0.3TMO at 180 K, and (d) 0.8BFO-0.2TMO at 180 K. XMCD signal was multiplied by 5 in all the cases for better visualization. Insets in (a) and (b) show the comparison of t_{2g} peak of L_3 edge and L_2 edge of the composites with standard α-Fe_2O_3, respectively.

mixed crystal coordination as the peaks are not shifted to the lower energy side, which should have been the case for mixed valence state.[57] From the XAS study, Fe ions are, thus, found to be in trivalent state with octahedral and another crystalline coordination.

The bottom panels of Figs. 8(a)–8(d) show the XMCD spectra of Fe ions of the composites 0.7BFO-0.3TMO and 0.8BFO-0.2TMO. The XMCD signal in the composite system is weak, and in Fig. 8, the XMCD signals are magnified five times for clear visualization. $BiFeO_3$ is antiferromagnetic at room temperature, and hence, it is not dichroic; thus, the absence of the XMCD signal of the composites at room temperature can be understood. Interestingly, the Fe XMCD spectrum at 180 K for the 0.8BFO-0.2TMO shows a clear dichroic signal similar to that of previously observed in γ-Fe_2O_3, BFO thin films, and La_2FeCrO_6.[51,58,59] It has been shown that in BFO weak ferromagnetism can be developed due to spin canting as a result of Dzyaloshinski-Moria interaction in the lattice. A similar XMCD spectrum has been reported by Kuo *et al.* to describe the weak ferromagnetism in $BiFeO_3$ thin films due to canted antiferromagnetic ordering.[58] Gray *et al.* have also shown similar Fe $L_{2,3}$ XMCD signal in the case of canted antiferromagnetic double perovskite La_2FeCrO_6.[59] In the case of γ-Fe_2O_3, the weak ferromagnetism arises as a result of alignment of spins of tetrahedral sites, which is canted in nature.[51,57] It is significant to mention here that in the *Pbnm* phase there are two sites available for Fe ions (O_h and T_d), whereas in the *R3c* phase, only O_h sites are available for Fe. Thus, the interfacial secondary *Pbnm* phase can also be responsible for the XMCD signal at the Fe edge of 0.8BFO-0.2TMO at 180 K. The dilute antiferromagnetic (2D DAFF) layer can be understood to be due to the interaction between Fe ions in the *Pbnm* phase, which was observed from the IRM measurements. The canting of Fe spins close

to the interface could arise due to the lattice strain at the interface as introduced by the TMO phase. This, however, should not affect the spin orientation further away from the interface. Kuo *et al.* have recently shown that the interfacial pinning plays a vital role in attaining the XMCD signal in Co/MnPc spinterface.[58] From the thickness dependent study of the layered structure, it has been shown that the XMCD signal varies when the pinning layer varies.[60] From the XMCD spectra at 300 K and 180 K, it can be conferred that as we decrease the temperature from 300 K, spin canting in the system increases in the system down to the spin reorientation temperature. From the ZFC-FC M-T study, it has been found that the system undergoes a spin reorientation transition like Morin transition observed in α-Fe_2O_3. Weak ferromagnetic behavior can be found above the transition due to canted antiferromagnetism, whereas the weak ferromagnetism vanishes below the transition. Thus, in our sample also, it is safe to assume that the system undergoes similar transition as has been observed in many $BiFeO_3$ based composite and materials. For canted antiferromagnetic ordering, there can be net magnetic moment in a particular direction. Thus, we can get an XMCD signal for a canted antiferromagnetic ordered sample. Therefore, we could get an XMCD signal above the spin reorientation transition, and there would be no signal below the transition. Thus, the XMCD signal can only be observed for 0.8BFO-0.2TMO composite at 180 K as the spin reorientation transition temperature ($T^* = 169$ K) is lower than 180 K, whereas it is ($T^* = 215$ K) higher than that of the XMCD measurement temperature (180 K) of 0.7BFO-0.3TMO.

Figures 9(a)–9(d) represent the Mn $L_{2,3}$-edge XAS and XMCD spectra of the two composites (0.7BFO-0.3TMO and 0.8BFO-0.2TMO) at 300 K and 180 K. The XAS spectra of the composites exhibit two broad spin-orbit split peaks of L_3 ($2P_{3/2}$) at ~641 eV and L_2 ($2P_{1/2}$) at ~652 eV separated by spin-orbit splitting energy ($\Delta E = \sim 11$ eV).

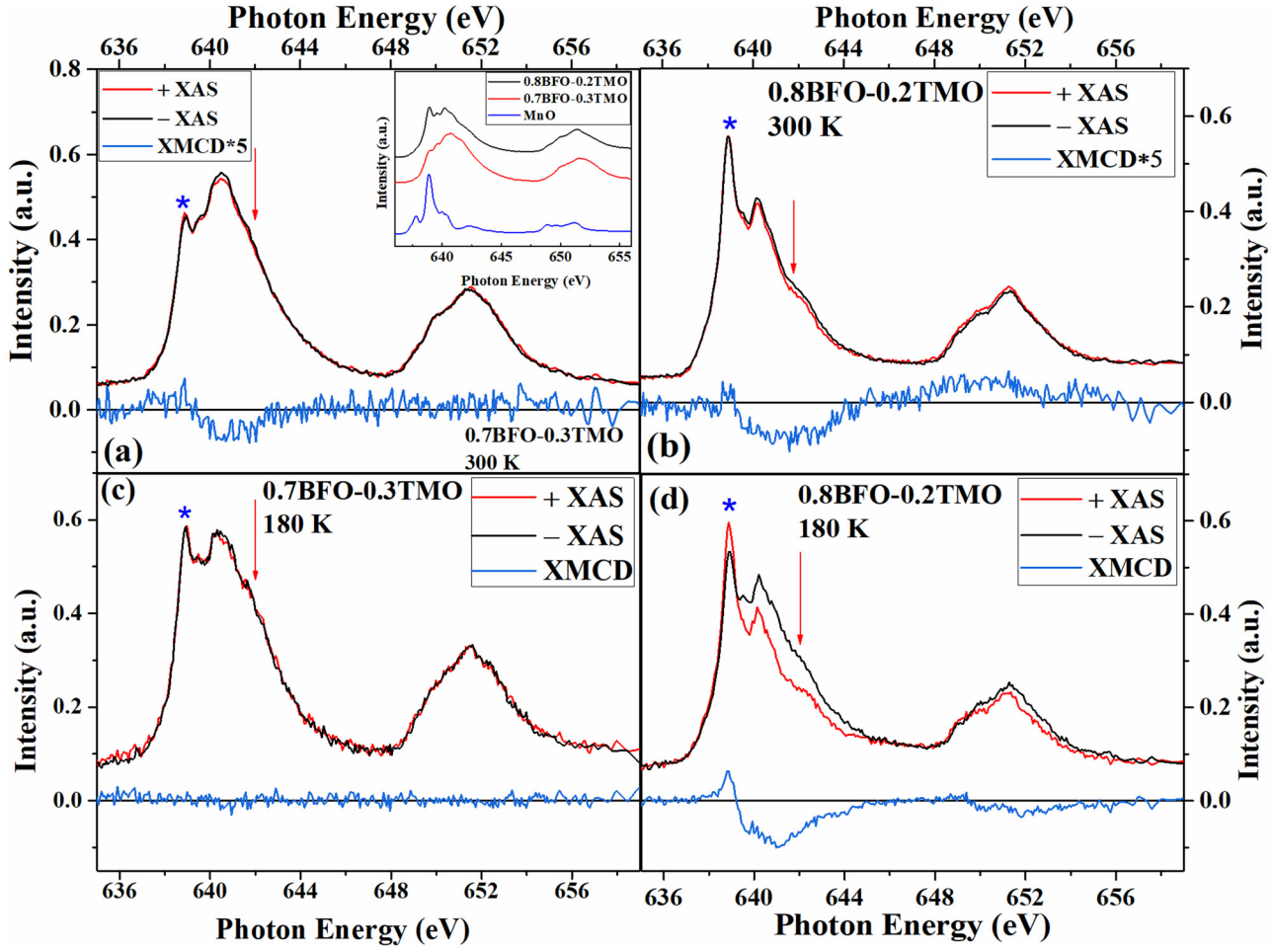

FIG. 9. Mn $L_{2,3}$ XAS and XMCD spectra of (a) 0.7BFO-0.3TMO at 300 K, (b) 0.8BFO-0.2TMO at 300 K, (c) 0.7BFO-0.3TMO at 180 K, and (d) 0.8BFO-0.2TMO at 180 K. XMCD signal was multiplied by 5 in case of (a) and (b) for better visualization. Inset in (a) shows the comparison between XAS spectra from 0.7BFO-0.3TMO, 0.8BFO-0.2TMO, and standard α-Fe_2O_3 sample.

The XAS spectra of the composites are compared with that of the standard MnO sample from which it can be easily concluded that the L_3 and L_2 peaks are shifted to higher energy side for the presence of higher valence state of Mn ions.[61] Interestingly, the composites show distinct behavior at L_3 and L_2 edges where the shape of the spectra does not match exactly with Mn_2O_3 in which Mn lies in the 3+ state, rather it matches well with Mn XAS spectra observed in $La_{0.7}Sr_{0.3}MnO_3$ thin films in which Mn lie in a mixed valence state.[53] The main peak observed at ~640 eV is due to the presence of Mn^{3+} as the position matches well with the Mn signal obtained from Mn_2O_3 in a tetragonally distorted D_{4h} crystal field and from TMO.[63,64] The high intensity peak $2P_{3/2}$ observed at ~640 eV shows distinct shoulder peaks at ~638 eV (marked by a blue star) and 642 eV (marked by a red arrow) indicating the existence of multivalent oxidation states of Mn. The spectral shape of any $L_{2,3}$ edge depends on different factors such as local crystal field effects, multiplet structure given by the Mn 3d-3d and 2p-3d Coulomb and exchange interactions, and the hybridization with the O2p ligands.[61] The peaks can be assigned to the presence of Mn^{2+} and Mn^{4+}, respectively, as has been done by several authors in Mn XAS spectra.[62,64–66] To maintain the charge neutrality, affected by oxygen vacancy present in the lattice, the mixed oxidation states can evolve in the system. The covalency can also arise from the charge transfer effect between the Mn3d orbitals and O2p ligand orbitals commonly observed in Mn based systems.[55] The valence instability of Mn^{3+} ions can also give rise to creation of Mn^{4+} and Mn^{2+} species, which is known to modify the bulk magnetic and electrical properties of different manganite systems.[64] Oxygen vacancies present in the composites, which is observed in the XPS analysis (not shown here) of the composite, can change the effective superexchange (SE) interaction between Mn ions. Yang *et al.* reported the change in the magnetic spin structure of $TbMnO_3$ due to the alternation in SE between next-nearest-neighbor Mn ions mediated through O ion.[67,68]

The XAS spectra of the 0.8BFO-0.2TMO [Figs. 9(b) and 9(d)] show more pronounced shoulder peaks due to the presence of Mn^{2+} and Mn^{4+} ions (marked by blue star and red arrow). From the spectra, it can be concluded that in this composite the 2+ state of the Mn ion dominated over other valence states. Moreover, the intensity ratio of the L_3 and L_2 (i.e., L_3/L_2) edges is also a significant parameter to determine the dominating oxidation states of transition metals (TMs) and their oxides with 3d occupancy.[69] For the transition metals that have d^0 to d^5 occupancy (i.e., up to half filled occupancy), the increment in the L_3/L_2 intensity ratio signifies reduction in the oxidation state of the TMs.[69,70] Larger L_3/L_2 intensity ratio for Mn ion in the 0.8BFO-0.2TMO composite than the other reveals that the dominating state of Mn is Mn^{2+}. The presence of large amount of Mn^{2+} and Mn^{4+} in this composite is understood to be due to the large lattice strain experienced by the TMO due to higher concentration of BFO in the 0.8BFO-0.2TMO composite. Lattice strain is known to create oxygen vacancies in a lattice, which, in turn, creates the mixed valence state of Mn ion in the composites.[71,72]

Mn $L_{3,2}$ edge XMCD signals of the composites are shown in the bottom panel of Figs. 9(a)–9(d). The room temperature XMCD signals have been multiplied by 5 for better visualization, which show very weak XMCD signal at L_3 and L_2 edges. Although the XMCD signals are weak and noisy at room temperature, XMCD peaks can be found in opposite polarity for Mn^{2+} with respect to that of Mn^{3+} and Mn^{4+} for both the composites, which shows the opposite alignment of Mn^{2+} ions with respect to Mn^{3+} and Mn^{4+}. Interestingly, the 180 K XMCD spectrum of 0.8BFO-0.2TMO shows prominent signal just like its Fe counterpart. The signal for Mn^{2+} is opposite in nature to the signal of Mn^{3+} and Mn^{4+} showing the antiferromagnetic coupling between them. Further, it is found that the magnitude of the Mn dichroism is almost diminished at 180 K for the composite 0.7BFO-0.3TMO due to the spin reorientation transition occurring at a higher temperature (225 K). This reduction of the Mn dichroism could be understood by taking into account spin reorientation transition near ~200 K observed from the magnetization measurement. Interestingly, the 180 K XAS signal of 0.7BFO-0.3TMO shows an increase in the intensity of the shoulder peak at ~638 eV, which signifies the increase in the charge transfer process between Mn ions at low temperature.

The contribution of spin moments and the orbital moments to XMCD signal are calculated following the XMCD sum rule.[73] Particularly, for the case of 0.8BFO-0.2TMO composite (for which a clear XMCD signal is observed), the spin and orbital momenta of Fe ions are calculated to be 0.09482 and 0.03477 μ_B/ion, respectively, and for that of Mn ions are 0.02181 and 0.07795 μ_B/ion. Clearly, the contribution of orbital moments is not negligible in these composites. This large orbital momentum can break the local symmetry in the proximity of the BFO/TMO interface, leading to strongly enhanced unidirectional anisotropy energy.[74] This local anisotropy energy is strong enough to induce effective exchange imbalance at the interface, which tries to rotate spin moments by spin-orbit coupling (SOC).[75] Recently, Nistor *et al.* have reported that the exchange bias in their system arises from the coupling of the Mn spins to the uncompensated spin at the interface.[75] Thus, in our sample also, there might be coupling of Mn spins to the uncompensated Fe spins at the interface. In addition to the coupling of Mn and Fe spins, there are also exchange coupling between Mn-Mn ions. This coupling of Mn-Mn and Mn-Fe ions would give rise to a layer of pinned magnetic moments at the interface. However, the detection and measurement of pinned magnetic moments cannot be done following the simple XMCD measurement protocol.[75]

Thus, analyzing XAS and XMCD spectra of all the $L_{3,2}$ edges, it can be concluded that charge transfer between Mn ions occurs due to oxygen vacancy and instability of the Mn^{3+} oxidation state. The charge transfer results in a mixed valence state of Mn ions in the composite. As a result of the transfer and mixed valence state of the TM ions, band gets reconstructed at the interface and the bandgap of the material is decreased.[50,76] The presence of mixed valence state creates different superexchange interaction between TM ions across the interface and in bulk. The result indicates the coupling of the Mn spins to the uncompensated spin of Fe, which forms a pinned layer of spin moments at the interface of the two components (BFO and TMO). This weak ferromagnetic layer is stabilized against the thermal fluctuations through exchange coupling to the 2D DAFF layer and/or to the core canted antiferromagnetic spins of BFO. On lowering the temperature from 300 K, the spin canting increases, as a result the uniaxial antiferromagnetic anisotropy decreases (seen from XMCD results). Thus, the exchange bias

is developed as a result of pinning of the interfacial ferromagnetic spins to the core antiferromagnetic BFO spins. Due to the dual phase structure of BFO, a thin layer of DAFF is formed at the skin of BFO core, which also favors the formation of canted antiferromagnetic ordering of the BFO lattice.

IV. CONCLUSION

In summary, we have studied the origin of exchange bias induced in $BiFeO_3$-$TbMnO_3$ composite (7:3 and 8:2 stoichiometric ratio) prepared via solid state reaction. In the prepared composite, $BiFeO_3$ has the rhombohedrally distorted perovskite (*R3c*) structure at the core and orthorhombically distorted *Pbnm* structure at the shell or skin, whereas $TbMnO_3$ has orthorhombically distorted perovskite (*Pbnm*) structure. We observed exchange bias at room temperature and low temperatures, which could not be explained on the basis of the pinning or a superspin glass state at low temperatures. Different models explaining the EB have been investigated, such as core-shell of hard and dilute antiferromagnet and charge transfer between Fe and Mn ions present at the interface of the two materials in the composite. The charge transfer between the Mn-Mn ions at the interface takes place due to the oxygen vacancy and instability of Mn^{3+} ions. The presence of a mixed charge state creates different exchange interactions between the TM ions (ferro and antiferromagnetic). The strong magnetoelectric coupling between the two components initiates canting and pinning of the interfacial BFO or TMO spins. From the IRM measurement, signatures of the presence of 2D dilute antiferromagnet have been found, which play a significant role in obtaining the exchange bias. The 2D DAFF layers are the result of the formation of the interfacial phase of BFO (*Pbnm*) in which the antiferromagnetic ordering is different from that of the *R3c* phase in the bulk; as a result the Fe edge shows γ-Fe_2O_3-like XMCD signal. The EB obtained at different temperatures also shows nonmonotonic variation with temperature. The decrease in AFM anisotropy due to spin canting and increase in FM ordering in the pinned layer with decrease in the temperature have been found to influence the temperature dependence of the EB. The role of interfacial pinning layer was invoked to influence the exchange bias in the system as indicated by the IRM results and XMCD spectra of Fe and Mn $L_{2,3}$ edges.

ACKNOWLEDGMENTS

The authors would like to acknowledge the Central Instrument Facility Centre of IIT (BHU) for the magnetic measurements.

REFERENCES

[1]W. H. Meiklejohn and C. P. Bean, "New magnetic anisotropy," Phys. Rev. **102**, 1413–1414 (1956).
[2]F. Tian, K. Cao, Y. Zhang, Y. Zeng, R. Zhang, T. Chang, C. Zhou, M. Xu, X. Song, and S. Yang, "Giant spontaneous exchange bias triggered by crossover of superspin glass in Sb-doped $Ni_{50}Mn_{38}Ga_{12}$ Heusler alloys," Sci. Rep. **6**, 30801 (2016).
[3]W. Echtenkamp and C. Binek, "Electric control of exchange bias training," Phys. Rev. Lett. **111**, 187204 (2013).
[4]M. Ali, P. Adie, C. H. Marrows, D. Greig, B. J. Hickey, and R. L. Stamps, "Exchange bias using a spin glass," Nat. Mater. **6**, 70–75 (2007).
[5]D. Navas, J. Torrejon, F. Béron, C. Redondo, F. Batallan, B. P. Toperverg, A. Devishvili, B. Sierra, F. Castaño, K. R. Pirota, and C. A. Ross, "Magnetization reversal and exchange bias effects in hard/soft ferromagnetic bilayers with orthogonal anisotropies," New J. Phys. **14**, 113001 (2012).
[6]T. Maity, S. Goswami, D. Bhattacharya, and S. Roy, "Superspin glass mediated giant spontaneous exchange bias in a nanocomposite of $BiFeO_3$-$Bi_2Fe_4O_9$," Phys. Rev. Lett. **110**, 107201 (2013).
[7]P. Fischer, M. Polomska, I. Sosnowska, and M. Szymanski, "Temperature dependence of the crystal and magnetic structures of $BiFeO_3$," J. Phys. C Solid State Phys. **13**, 1931–1940 (1980).
[8]T.-J. Park, G. C. Papaefthymiou, A. J. Viescas, A. R. Moodenbaugh, and S. S. Wong, "Size-dependent magnetic properties of single-crystalline multiferroic $BiFeO_3$ nanoparticles," Nano Lett. **7**, 766–772 (2007).
[9]S. H. Xie, J. Y. Li, R. Proksch, Y. M. Liu, Y. C. Zhou, Y. Y. Liu, Y. Ou, L. N. Lan, and Y. Qiao, "Nanocrystalline multiferroic $BiFeO_3$ ultrafine fibers by sol-gel based electrospinning," Appl. Phys. Lett. **93**, 222904 (2008).
[10]X. Q. Xu, T. Qian, G. Q. Zhang, T. Zhang, G. Li, W. Wang, and X. G. Li, "Fabrication and magnetic properties of multiferroic $BiFeO_3$ nanotube arrays," Chem. Lett. **36**, 112–113 (2007).
[11]S. Dong, Y. Yao, Y. Hou, Y. Liu, Y. Tang, and X. Li, "Dynamic properties of spin cluster glass and the exchange bias effect in $BiFeO_3$ nanocrystals," Nanotechnology **22**, 385701 (2011).
[12]P. K. Manna, S. M. Yusuf, R. Shukla, and A. K. Tyagi, "Exchange bias in $BiFe_{0.8}Mn_{0.2}O_3$ nanoparticles with an antiferromagnetic core and a diluted antiferromagnetic shell," Phys. Rev. B **83**, 184412 (2011).
[13]M. J. Calderón, S. Liang, R. Yu, J. Salafranca, S. Dong, S. Yunoki, L. Brey, A. Moreo, and E. Dagotto, "Magnetoelectric coupling at the interface of $BiFeO_3$/$La_{0.7}Sr_{0.3}MnO_3$ multilayers," Phys. Rev. B **84**, 024422 (2011).
[14]T. Maity, S. Goswami, D. Bhattacharya, G. C. Das, and S. Roy, "Spontaneous exchange bias in a nanocomposite of $BiFeO_3$-$Bi_2Fe_4O_9$," J. Appl. Phys. **113**, 17D916 (2013).
[15]B. Ahmmad, M. Z. Islam, A. Billah, and M. A. Basith, "Anomalous coercivity enhancement with temperature and tunable exchange bias in Gd and Ti co-doped $BiFeO_3$ multiferroics," J. Phys. D Appl. Phys. **49**, 095001 (2016).
[16]C. Zhang, S. Y. Wang, W. F. Liu, X. L. Xu, X. Li, H. Zhang, J. Gao, and D. J. Li, "Room temperature exchange bias in multiferroic $BiFeO_3$ nano-and microcrystals with antiferromagnetic core and two-dimensional diluted antiferromagnetic shell," J. Nanopart. Res. **19**, 182 (2017).
[17]C. Djurberg, P. Svedlindh, P. Nordblad, M. F. Hansen, F. Bødker, and S. Mørup, "Dynamics of an interacting particle system: Evidence of critical slowing down," Phys. Rev. B **79**, 5154 (1997).
[18]W. Kleemann, O. Petracic, C. Binek, G. N. Kakazei, Y. G. Pogorelov, J. B. Sousa, S. Cardoso, and P. P. Freitas, "Interacting ferromagnetic nanoparticles in discontinuous $Co_{80}Fe_{20}$/Al_2O_3 multilayers: From superspin glass to reentrant superferromagnetism," Phys. Rev. B **63**, 134423 (2001).
[19]X. Martí, P. Ferrer, J. H. Albillos, J. Narvaez, V. Holy, N. Barrett, M. Alexe, and G. Catalan, "Skin layer of $BiFeO_3$ single crystals," Phys. Rev. Lett. **106**, 236101 (2011).
[20]L. W. Martin, Y. H. Chu, Q. Zhan, and R. Ramesh, "Room temperature exchange bias and spin valves based on $BiFeO_3$/$SrRuO_3$/$SrTiO_3$/Si (001) heterostructures," Appl. Phys. Lett. **91**, 172513 (2007).
[21]M. Lorenz, V. Lazenka, P. Schwinkendorf, F. Bern, M. Ziese, H. Modarresi, A. Volodin, M. J. Van Bael, K. Temst, A. Vantomme, and M. Grundmann, "Multiferroic $BaTiO_3$–$BiFeO_3$ composite thin films and multilayers: Strain engineering and magnetoelectric coupling," J. Phys. D Appl. Phys. **47**, 135303 (2014).
[22]T. Kimura, T. Goto, H. Shintani, K. Ishizaka, T. Arima, and Y. Tokura, "Magnetic control of ferroelectric polarization," Nature **426**, 55–58 (2003).
[23]A. Kumar, P. Shahi, S. Kumar, K. K. Shukla, R. K. Singh, A. K. Ghosh, A. K. Nigam, and S. Chatterjee, "Raman effect and magnetic properties of doped $TbMnO_3$," J. Phys. D Appl. Phys. **46**, 125001 (2013).

[24]R. Haumont, P. Bouvier, A. Pashkin, K. Rabia, S. Frank, B. Dkhil, W. A. Crichton, C. A. Kuntscher, and J. Kreisel, "Effect of high pressure on multiferroic $BiFeO_3$," Phys. Rev. B **79**, 184110 (2009).
[25]F. Kubel and H. Schmid, "Structure of a ferroelectric and ferroelastic monodomain crystal of the perovskite $BiFeO_3$," Acta Cryst. B **46**, 698 (1990).
[26]A. Malashevich and D. Vanderbilt, "First principles study of improper ferroelectricity in $TbMnO_3$," Phys. Rev. Lett. **101**, 037210 (2008).
[27]A. A. Belik, A. M. Abakumov, A. A. Tsirlin, J. Hadermann, J. Kim, G. Van Tendeloo, and E. T. Muromachi, "Structure and magnetic properties of $BiFe_{0.75}Mn_{0.25}O_3$ perovskite prepared at ambient and high pressure," Chem. Mater. **23**, 4505–4514 (2011).
[28]J. Walker, H. Simons, D. O. Alikin, A. P. Turygin, V. Y. Shur, A. L. Kholkin, H. Ursic, A. Bencan, B. Malic, V. Nagarajan, and T. Rojac, "Dual strain mechanisms in a lead free morphotropic phase boundary ferroelectric," Sci. Rep. **6**, 19630 (2016).
[29]A. Lahmar and M. Es-souni, "Sequence of structural transitions in $BiFeO_3$–$RMnO_3$ thin films (R = rare earth)," Ceram. Int. **41**, 5721–5726 (2015).
[30]S. N. Tripathy, D. K. Pradhan, K. K. Mishra, S. Sen, R. Palai, M. Paulch, J. F. Scott, R. S. Katiyar, and D. K. Pradhan, "Phase transition and enhanced magneto-dielectric response in $BiFeO_3$-$DyMnO_3$ multiferroics," J. Appl. Phys. **117**, 144103 (2015).
[31]S. N. Tripathy, K. K. Mishra, S. Sen, B. G. Mishra, D. K. Pradhan, R. Palai, and D. K. Pradhan, "Phase transition and magneto-electric coupling of $BiFeO_3$–$YMnO_3$ multiferroic nanoceramics," J. Appl. Phys. **114**, 144104 (2013).
[32]G. S. Lotey and N. Verma, "Magnetoelectric coupling in multiferroic Tb-doped $BiFeO_3$ nanoparticles," Mater. Lett. **111**, 55–58 (2013).
[33]R. D. Shannon and C. T. Prewitt, "Effective ionic radii of oxides and fluorides," Acta Crystallogr. B **25**, 925–946 (1969).
[34]H. Wu, J. Zhou, L. Liang, L. Li, and X. Zhu, "Fabrication, characterization, properties, and applications of low-dimensional $BiFeO_3$ nanostructures," J. Nanomater. **2014**, 471485.
[35]S. A. Acharya, S. M. Khule, and V. M. Gaikwad, "Investigation of multiferroic behaviour of $TbMnO_3$nanoplates," Mater. Res. Bull. **67**, 111–117 (2015).
[36]N. Srivastava and P. C. Srivastava, "A study on exchange coupled structures of Fe/NiO and NiO/Fe interfaced with n- and p-silicon substrates," J. Appl. Phys. **111**, 123909 (2012).
[37]O. P. Bajpai, S. Mandal, R. Ananthakrishnan, P. Mandal, D. Khastgir, and S. Chattopadhyay, "Structural features, magnetic properties and photocatalytic activity of bismuth ferrite nanoparticles grafted on graphene nanosheets," New J. Chem. **42**, 10712–10723 (2018).
[38]M. Ranjbar, S. N. Piramanayagam, R. Sbiaa, T. C. Chong, and I. Okamoto, "Advanced magnetic force microscopy for high resolution magnetic imaging," Nanosci. Nanotechnol. Lett. **4**, 628–633 (2012).
[39]M. K. Singh, R. S. Katiyar, and J. F. Scott, "New magnetic phase transitions in $BiFeO_3$," J. Phys. Condens. Matter **20**, 252203 (2008).
[40]S. Bhattacharya, A. Senyshyn, H. Fuess, and D. Pandey, "Morin-type spin-reorientation transition below the Néel transition in the monoclinic compositions of $(1-x)BiFeO_3$-$xPbTiO_3$ (x = 0.25 and 0.27): A combined dc magnetization and x-ray and neutron powder diffraction study," Phys. Rev. B **87**, 054417 (2013).
[41]A. Kumar, and D. Pandey, e-print arXiv:1606.06075v1 (2016).
[42]F. J. Morin, "Electrical properties of αFe_2O_3 and αFe_2O_3 containing titanium," Phys. Rev. **83**, 1005 (1951).
[43]T. G. Worlton and D. L. Decker, "Neutron diffraction study of the magnetic structure of hematite to 41 kbar," Phys. Rev. **171**, 596 (1968).
[44]Y. Wang, J. Hu, Y. Lin, and C.-W. Nan, "Multiferroic magnetoelectric composite nanostructures," NPG Asia Mater. **2**, 61–68 (2010).
[45]M. J. Benitez, O. Petracic, H. Tuysuz, F. Schuth, and H. Zabel, "Fingerprinting the magnetic behavior of antiferromagnetic nanostructures using remanent magnetization curves," Phys. Rev. B **83**, 134424 (2011).
[46]S. Fishman and A. Aharony, "Random field effects in disordered anisotropic antiferromagnet," J. Phys. C Solid State Phys. **12**, L729 (1979).
[47]A. Aharony, A. B. Harris, and Y. Meir, "Dilute random-field Ising models and uniform-field antiferromagnets," Phys. Rev. B **32**, 3203 (1985).
[48]A. Hoffmann, "Symmetry driven irreversibilities at ferromagnetic-antiferromagnetic interfaces," Phys. Rev. Lett. **93**, 097203 (2004).
[49]J. Goodenough, *Magnetism and the Chemical Bond* (John Wiley and Sons, New York, 1963).
[50]P. Yu, Y. H. Chu, and R. Ramesh, "Emergent phenomena at multiferroic heterointerfaces," Philos. Trans. R. Soc. A **370**, 4856–4871 (2012).
[51]D. H. Kim, H. J. Lee, G. Kim, Y. S. Koo, J. H. Jung, H. J. Shin, J.-Y. Kim, and J.-S. Kang, "Interface electronic structures of $BaTiO_3$@X nanoparticles (X = γ-Fe_2O_3, Fe_3O_4, α-Fe_2O_3, and Fe) investigated by XAS and XMCD," Phys. Rev B **79**, 033402 (2009).
[52]Q. Xu, Y. Sheng, M. Khalid, Y. Cao, Y. Wang, X. Qiu, W. Zhang, M. He, S. Wang, S. Zhou, Q. Li, D. Wu, Y. Zhai, W. Liu, P. Wang, Y. B. Xu, and J. Du, "Magnetic interactions in $BiFe_{0.5}Mn_{0.5}O_3$ films and $BiFeO_3$/$BiMnO_3$superlattices," Sci. Rep. **5**, 9093 (2015).
[53]H. Béa, M. Bibes, S. Cherifi, F. Nolting, B. Warot-Fonrose, S. Fusil, G. Herranz, C. Deranlot, E. Jacquet, K. Bouzehouane, and A. Barthélémy, "Tunnel magnetoresistance and robust room temperature exchange bias with multiferroic $BiFeO_3$ epitaxial thin films," Appl. Phys. Lett. **89**, 242114 (2006).
[54]M. Abbate, F. M. F. de Groot, J. C. Fuggle, A. Fujimori, O. Strebel, F. Lopez, M. Domke, G. Kaindl, G. A. Sawatzky, M. Takano, Y. Takeda, H. Eisaki, and S. Uchida, "Controlled-valence properties of $La_{1-x}Sr_xFeO_3$ and $La_{1-x}Sr_xMnO_3$ studied by soft-I-ray absorption spectroscopy," Phys. Rev. B **46**, 4511–4519 (1992).
[55]J. S. Kang, H. J. Lee, G. Kim, D. H. Kim, B. Dabrowski, S. Kolesnik, H. Lee, J.-Y. Kim, and B. I. Min, "Electronic structure of the cubic perovskite $SrMn_{1-x}Fe_xO_3$ investigated by x-ray spectroscopies," Phys. Rev. B **78**, 054434 (2008).
[56]J.-S. Kang, J. Hwang, D. H. Kim, E. Lee, W. C. Kim, C. S. Kim, S. Kwon, S. Lee, J.-Y. Kim, T. Ueno, M. Sawada, B. Kim, B. H. Kim, and B. H. Min, "Valence states and spin structure of spinel FeV_2O_4 with different orbital degrees of freedom," Phys. Rev. B **85**, 165136 (2012).
[57]T. J. Regan, H. Ohldag, C. Stamm, F. Nolting, J. Lüning, J. Stöhr, and R. L. White, "Chemical effects at metal oxide interfaces studied by x-ray-absorption spectroscopy," Phys. Rev. B **64**, 214422 (2001).
[58]C.-Y. Kuo, Z. Hu, J. C. Yang, S. C. Liao, Y. L. Huang, R. K. Vasudevan, M. B. Okatan, S. Jesse, S. V. Kalinin, L. Li *et al.*, "Single-domain multiferroic $BiFeO_3$ films," Nat. Commun. **7**, 12712 (2016).
[59]B. Gray, H. N. Lee, J. Liu, J. Chakhalian, and J. W. Freeland, "Local electronic and magnetic studies of an artificial La_2FeCrO_6 double perovskite," Appl. Phys. Lett. **97**, 013105 (2010).
[60]M. Gruber, F. Ibrahim, S. Boukari, H. Isshiki, L. Joly, M. Peter, M. Studniarek, V. Da Costa, H. Jabbar, V. Davesne *et al.*, "Exchange bias and room-temperature magnetic order in molecular layers," Nat. Mater. **14**, 981 (2015).
[61]H. Guo, A. Gupta, M. Varela, S. Pennycook, and J. Zhang, "Local valence and magnetic characteristics of La_2NiMnO_6," Phys. Rev. B **79**, 172402 (2009).
[62]M. S. Kim, J. B. Yang, Q. Cai, X. D. Zhou, W. J. James, W. B. Yelon, P. E. Parris, D. Buddhikot, and S. K. Malik, "Structure, magnetic, and transport properties of Ti-substituted $La_{0.7}Sr_{0.3}MnO_3$," Phys. Rev. B **71**, 014433 (2005).
[63]C. Mitra, Z. Hu, P. Raychaudhuri, S. Wirth, S. I. Csiszar, H. H. Hsieh, H.-J. Lin, C. T. Chen, and L. H. Tjeng, "Direct observation of electron doping in $La_{0.7}Ce_{0.3}MnO_3$ using x-ray absorption spectroscopy," Phys. Rev. B **67**, 092404 (2003).
[64]V. Cuartero, S. Lafuerza, G. Subías, J. García, E. Schierle, J. Blascoand, and J. Herrero-Albillos, "X-ray magnetic circular dichroism study of the magnetic anisotropy on $TbMnO_3$," Phys. Rev. B **91**, 165111 (2015).
[65]B. B. Nelson-Cheeseman, F. J. Wong, R. V. Chopdekar, E. Arenholz, and Y. Suzuki, "Room temperature magnetic barrier layers in magnetic tunnel junctions," Phys. Rev. B **81**, 214421 (2010).
[66]G. D. Dwivedi, A. G. Joshi, S. Kumar, H. Chou, K. S. Yang, D. J. Jhong, W. L. Chan, A. K. Ghosh, and S. Chatterjee, "Electronic structure study of wide band gap magnetic semiconductor $(La_{0.6}Pr_{0.4})_{0.65}Ca_{0.35}MnO_3$ nanocrystals in paramagnetic and ferromagnetic phases," Appl. Phys. Lett. **108**, 172402 (2016).

[67]C. C. Yang, M. K. Chung, W. H. Li, T. S. Chan, R. S. Liu, Y. H. Lien, C. Y. Huang, Y. Y. Chan, Y. D. Yao, and J. W. Lynn, "Magnetic instability and oxygen deficiency in Na-doped $TbMnO_3$," Phys. Rev. B **74**, 094409 (2006).
[68]C. C. Yang, C.-M. Wu, W.-H. Li, T. S. Chan, R. S. Liu, Y. Y. Chen, and M. Avdeev, "Effects of oxygen deficiency on the magnetic ordering of Mn in $Tb_{0.9}Na_{0.1}MnO_{2.9}$," J. Phys. Condens. Matter **20**, 104234 (2008).
[69]J. Graetz, C. C. Ahn, H. Ouyang, P. Rez, and B. Fultz, "White lines and d-band occupancy for the 3d transition-metal oxides and lithium transition-metal oxides," Phys. Rev. B **69**, 235103 (2004).
[70]F. Lin, D. Nordlund, T. Pan, I. M. Markus, T.-C. Weng, H. L. Xin, and M. M. Doeff, "Influence of synthesis conditions on the surface passivation and electrochemical behavior of layered cathode materials," J. Mater. Chem. A **2**, 19833–19840 (2014).
[71]D. Ma, Z. Lu, Y. Tang, T. Li, Z. Tang, and Z. Yang, "Effect of lattice strain on the oxygen vacancy formation and hydrogen adsorption at CeO_2(111) surface," Phys. Lett. A **378**, 2570–2575 (2014).
[72]J. R. Petrie, C. Mitra, H. Jeen, W. S. Choi, T. L. Meyer, F. A. Reboredo, J. W. Freeland, G. Eres, and H. N. Lee, "Strain control of oxygen vacancies in epitaxial strontium cobaltite films," Adv. Funct. Mater. **26**, 1564–1570 (2016).
[73]P. Carra, B. T. Thole, M. Altarelli, and X. Wang, "X-ray circular dichroism and local magnetic fields," Phys. Rev. Lett. **70**, 694–697 (1993).
[74]P. Audehm, M. Schmidt, S. Bruck, T. Tietze, J. Grafe, S. Macke, G. Schütz, and E. Goering, "Pinned orbital moments—A new contribution to magnetic anisotropy," Sci. Rep. **6**, 25517 (2016).
[75]C. Nistor, C. Krull, A. Mugarza, S. Stepanow, C. Stamm, M. Soares, S. Klyatskaya, M. Ruben, and P. Gambardella, "Exchange bias of $TbPc_2$ molecular magnets on antiferromagnetic FeMn and ferromagnetic Fe films," Phys. Rev. B **92**, 184402 (2015).
[76]P. Yu, J. S. Lee, S. Okamoto, M. D. Rossell, M. Huijben, C. H. Yang, Q. He, J. X. Zhang, S. Y. Yang, M. J. Lee, Q. M. Ramasse, R. Erni, Y. H. Chu, D. A. Arena, C. C. Kao, L. W. Martin, and R. Ramesh, "Interface ferromagnetism and orbital reconstruction in $BiFeO_3$-$La_{0.7}Sr_{0.3}MnO_3$ heterostructures," Phys. Rev. Lett. **105**, 027201 (2010).